FEM model for analysis of RC prestressed thin-walled beams

M. Bottoni, C. Mazzotti & M. Savoia
DISTART - Structural Engineering, University of Bologna, Bologna, Italy

ABSTRACT: This paper deals with service behavior of prestressed cracked thin-walled beams. A non linear finite element model for thin-walled beams has been developed. Deflections in the non-linear range are obtained by adopting a smeared crack model for concrete in tension. Contribution of steel bars in reducing deformation has been considered. An example of a thin-walled prestressed girder is presented.

1 INTRODUCTION

Microcracking and cracking have a strong influence on instantaneous and long-term behaviour of concrete (Ghali & Favre 1994). Adoption of constitutive law for concrete in his cracked state is essential and mandatory to describe structural deformability under service loads. Another important phenomenon for structures during their service life is creep deformation, which can cause deflections two or three times greater then instantaneous counterpart (Bažant 1988, Favre et al. 1997).

Service behaviour of reinforced concrete is particularly important for some kinds of structures such as bridges or roof girders, due to their large spans and small thicknesses, increasing deformation and creep effects. For these structural elements, warping effects may be very significant and traditional beam models do not apply properly; theories for thin-walled beams are much more appropriate (see Laudiero & Savoia 1990, Capuani et al. 1998, Prokič 1996, Prokič 2002).

In the present paper, a non-linear finite element model is presented for the analysis of deformability of reinforced concrete thin-walled beams.

A finite element formulation for thin-walled beams is firstly introduced (see also Bottoni et al. 2006); the kinematic model is described and equations derived from FE discretization are given. Main assumption is that of cross-sections rigid in their own planes; this hypothesis reduces the total number of dofs involved in the analysis and, correspondingly, computational effort. Furthermore, it is acceptable for analysis of beams under service loadings. On the contrary, longitudinal displacements are obtained through dofs in the section plane, so allowing for warping or shear-lag effects. Longitudinal displacement is considered constant within the thickness. The resulting finite element is essentially a membrane element with null deformation along the transverse axis. The presence of ordinary or prestressed steel reinforcement is considered through homogenization over the thickness.

As far as material modelization is concerned, a smeared crack approach is adopted for concrete, providing the average behaviour under tension after cracking. Ordinary steel reinforcement is modelled as layers of different materials in the finite element, whereas prestressed steel strands are modelled as separate panels.

Solution algorithm in the non-linear range is developed, adopting a displacement-control method as proposed by Batoz & Dhatt (1979).

Finally, an example of a roof precast and prestressed RC element is reported. Results are given in term of load-deflection curves, strains and stresses distributions as well as concrete cracking maps.

2 THE FINITE ELEMENT MODEL

2.1 *Kinematic model*

The kinematic model is defined according to the reference system shown in Figure 1, where a prismatic reinforced concrete thin-walled beam is depicted; each branch of the cross-section can be constituted by different materials through-the-thickness, in order to consider the presence of reinforcement steel.

A global right-handed orthogonal coordinate system $(O; x, y, z)$ is adopted, where x- and y- are two general axes belonging to the cross-section plane. Location of the reference system origin O and direction of x- and y-axes are general, i.e. they do not
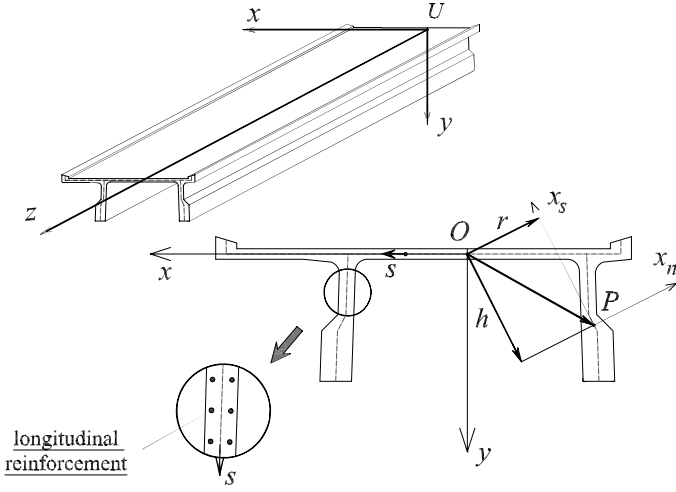
Figure 1. Thin-walled beam and its general cross-section.

necessarily coincide with centroid (or shear centre) and principal axes of the cross section. Coordinates of general point P can be expressed as:

$$x = x(s), \quad y = y(s) \tag{1}$$

where s is a curvilinear coordinate lying on the profile centerline. At any general point P of section contour, a local right-handed orthogonal coordinate system $(P; x_s, x_n, z)$ is also defined (Fig. 1), where x_s- and x_n- axes, lying in the section plane, are tangential and orthogonal to the centerline, respectively.

Together with the definition of a reference system, the kinematic model is based upon the following main assumptions:
a) Thickness of various branches constituting the cross-section is small with respect to overall cross-section dimensions;
b) Cross-sections are rigid in their own planes;
c) Displacements along z-direction are independent from cross-section in-plane displacements;
d) No variation of kinematic or static variables across the thickness is considered.

According to hypothesis b), in-plane displacements of point P are defined through rigid movements of the cross-section itself; therefore, they can be expressed as a function of displacement components $\xi(z)$ and $\eta(z)$ of O along x- and y-axes and of $\theta(z)$, cross-section rotation around O (Fig. 2).

According to hypothesis c), $w(s,z)$ is the displacement along the longitudinal axis z and it is independent from other displacement components. Accordingly, displacements of general point $P(s,z)$ along x–, y– and z–directions are, respectively (Bottoni et al. 2006):

$$u(s,z) = \xi(z) - y\,\theta(z) \tag{2a}$$

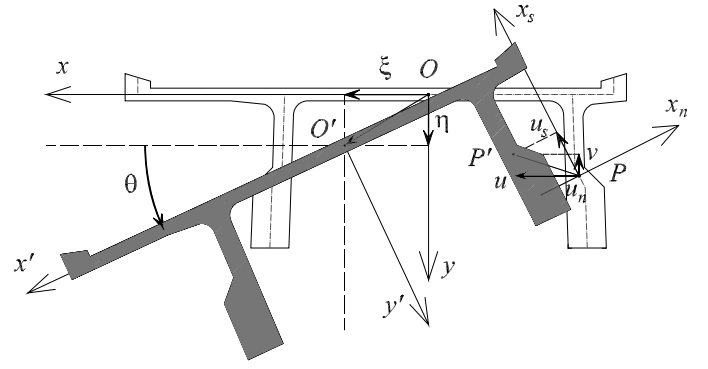$$v(s,z) = \eta(z) + x\,\theta(z) \tag{2b}$$

$$w = w(s,z) \tag{2c}$$

Figure 2. Displacement components in global and local reference systems.

By geometrical considerations, displacements of point $P(s,z)$ along local coordinate axes x_n, x_s can be expressed as:

$$u_n(s,z) = \xi(z)\frac{dy(s)}{ds} + \eta(z)\frac{dx(s)}{ds} - h(s)\theta(z) \tag{3a}$$

$$u_s(s,z) = \xi(z)\frac{dx(s)}{ds} + \eta(z)\frac{dy(s)}{ds} + r(s)\theta(z) \tag{3b}$$

respectively, where $r(s)$ and $h(s)$ are components along x_n, x_s of vector OP, i.e. (see Fig 1):

$$r(s) = x(s)\frac{dy(s)}{ds} - y(s)\frac{dx(s)}{ds} \tag{4a}$$

$$h(s) = x(s)\frac{dx(s)}{ds} + y(s)\frac{dy(s)}{ds} \tag{4b}$$

2.2 Strain and stress components

From Equations 3, strain components ε_z, γ_{zs}, γ_{zn} can be written as:

$$\varepsilon_z(s,z) = \frac{\partial w(s,z)}{\partial z} \tag{5a}$$

$$\gamma_{zs}(s,z) = \frac{\partial w}{\partial s} + \frac{\partial u_s}{\partial z} = \frac{\partial w}{\partial s} + \left(\frac{dx}{ds}\frac{d\xi}{dz} + \frac{dy}{ds}\frac{d\eta}{dz} + r\frac{d\theta}{dz}\right) \tag{5b}$$

According to hypothesis d) of section 2.1, strain components are constant across wall thickness. Moreover, due to small wall thickness, strain component γ_{zn} can be neglected. Finally, strain components ε_s, ε_n, e γ_{ns} are zero due to hypothesis b) of rigid cross-sections.

Shear strain γ_{zs}^{SV}, corresponding to Saint Venant torsion and linearly varying across wall thickness with null value on the centerline, is then superimposed to shear strain defined in Equation 5b. This strain component cannot be derived rigorously from displacement field described by Equations 2, due to the assumption of constant axial displacement through-the-thickness. However, Saint-Venant stiff-

ness is essential for open thin-walled beams to withstand uniform torsion. Corresponding strain γ_{zs}^{SV} is assumed to be proportional to the derivative of the torsion angle θ with respect to longitudinal axis z, according to the expression (Laudiero & Zaccaria 1988):

$$\gamma_{zs}^{SV} = 2\frac{d\theta(z)}{dz}x_n \qquad (6)$$

The model can be further simplified by making assumptions on stress components. First of all, due to the assumption of rigid cross-section, in-plane normal and shear stresses (σ_s, σ_n, τ_{ns}) cannot be determined explicitly, but they are negligible with respect to other components.

Moreover, due to small thickness of thin-walled beam, shear stress τ_{zn} is also negligible. Hence, only stresses σ_z and τ_{zs} are considered in the present model, together with shear stress τ_{zs}^{SV}. Stress components are related to corresponding strains through constitutive laws, i.e.:

$$\sigma_z^i = E_z^i \varepsilon_z \qquad (7a)$$

$$\tau_{zs}^i = G_{zs}^i \gamma_{zs} \qquad (7b)$$

$$\tau_{zs}^{SV,i} = G_{zs}^i \gamma_{zs}^{SV} \qquad (7c)$$

where superscript i refers to i-th layer and E_z and G_{zs} are secant values (in non linear range) of longitudinal Young modulus and transverse shear modulus, respectively. Considering different materials through the wall thickness, corresponding stress components, σ_z, τ_{zs} and τ_{zs}^{SV}, are obtained through individual constitutive laws.

3 NUMERICAL MODEL

3.1 *The finite element model*

The application of the finite element method requires a proper discretization of geometric domain. In the proposed model, discretization is performed following two main phases: first, thin-walled beam is divided along the longitudinal direction in subelements, by using a number of reference cross sections; secondly, general transverse cross-section is discretized into a number of straight segments defined between couples of nodes (Fig. 3). Nodes are forced to be located where some kind of discontinuity arises: geometrical discontinuity (first derivative of curvilinear coordinate and wall thickness), material discontinuity and where three or more walls intersect each other. Additional intermediate nodes are also considered in order to improve the solution. Joining the corresponding nodes of different transverse sections, a nodal line is obtained. The single
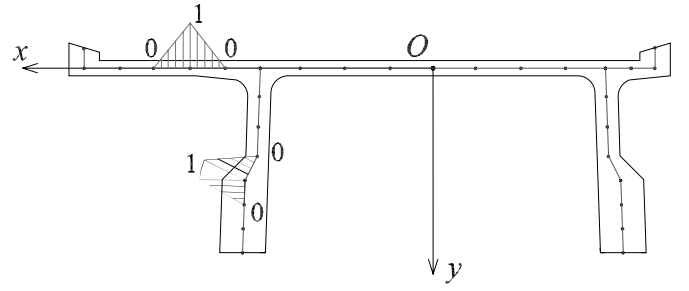

Figure 3. Nodes on transverse cross-section and linear approximation for axial displacements.

finite element, called *panel*, is defined as the portion of wall between two adjacent sections and two adjacent nodal lines (Fig. 4). A linear variation of longitudinal displacement $w(s,z)$ is considered along the cross-section curvilinear coordinate s, whereas quadratic approximation is adopted along z-direction (Bottoni et al. 2006).

Moreover, quadratic functions are used for in-plane cross-sectional displacements $\xi(z)$, $\eta(z)$, $\theta(z)$. The resulting finite element has 6 nodes and 15 dofs (Fig. 5): 6 for axial displacements and 9 for rigid body transverse displacements of three involved cross-sections.

All finite elements whose edges are located in a common transverse section share the same rigid body displacements. Hence, displacement functions providing rigid body displacements of cross-sections can be written in the form:

$$\xi(z) = \mathbf{N}^T(z)\boldsymbol{\xi} \qquad (8a)$$

$$\eta(z) = \mathbf{N}^T(z)\boldsymbol{\eta} \qquad (8b)$$

$$\theta(z) = \mathbf{N}^T(z)\boldsymbol{\theta} \qquad (8c)$$

where vectors:

$$\boldsymbol{\xi}^T = [\xi_1, \xi_2, \xi_3], \quad \boldsymbol{\eta}^T = [\eta_1, \eta_2, \eta_3],$$

$$\boldsymbol{\theta}^T = [\theta_1, \theta_2, \theta_3] \qquad (9)$$

contain rigid body dofs while vector $\mathbf{N}^T=[N_1, N_2, N_3]$ contains quadratic shape functions. Moreover, axial displacement is given by:

$$w(s,z) = \mathbf{N}_\phi^T(s,z)\boldsymbol{\Phi} \qquad (10)$$

where vector:

$$\boldsymbol{\Phi}^T = [\phi_{11}, \phi_{12}, \phi_{13}, \phi_{21}, \phi_{22}, \phi_{23}] \qquad (11)$$

contains axial dofs, while shape functions collected in vector $\mathbf{N}_\phi^T(s,z)$ are defined by the composition of $\mathbf{N}(z)$ and linear Lagrangean interpolation functions $\mathbf{M}^T(s)=[M_1(s), M_2(s)]$ according to expression:

$$\mathbf{N}_\phi^T(s,z) = [M_1(s)\cdot\mathbf{N}^T(z), M_2(s)\cdot\mathbf{N}^T(z)] \qquad (12)$$
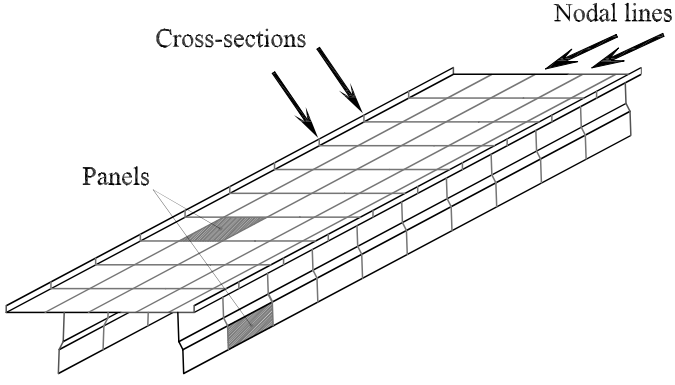
Figure 4. Discretization of the beam. Longitudinal and cross-sectional subdivision.

From Equations 5, 8, strain components can then be written as:

$$\varepsilon_z(s,z) = \frac{\partial w(s,z)}{\partial z} = \mathbf{N}_\phi'^T(s,z)\Phi \tag{13a}$$

$$\gamma_{zs}(s,z) = \frac{\partial u_s(s,z)}{\partial z} + \frac{\partial w(s,z)}{\partial s} =$$
$$= \alpha_x \mathbf{N}'^T(z)\xi + \alpha_y \mathbf{N}'^T(z)\eta + \tag{13b}$$
$$+ r\mathbf{N}'^T(z)\theta + \mathbf{N}_{\phi,s}^T(s,z)\Phi$$

where prime stands for partial derivative with respect to z and coefficients $\alpha_x = dx/ds$, $\alpha_y = dy/ds$, $r = xdy - ydx$ are constant for each finite element.
Finally, Saint Venant shear strains are given by (see Equation 6):

$$\gamma_{zs}^{SV}(s,z) = 2\theta'(z)x_n = 2\mathbf{N}'(z)\theta\, x_n \tag{14}$$

3.2 Equilibrium conditions for the finite element

Equilibrium conditions for the single finite element can be written by the principle of virtual displacements. Making use of Equations 5, 6 and 7, inner virtual work can be written as:

$$\delta L_{vi}^e = \int_{V_e} (\sigma_z \,\delta\varepsilon_z + \tau_{zs}\,\delta\gamma_{zs} + \tau_{zs}^{SV}\,\delta\gamma_{zs}^{SV})\,dV_e =$$
$$= t_e \int_{H_e}\int_{L_e}\big(\delta\varepsilon_z E_z^{eq}\varepsilon_z + \delta\gamma_{zs}G_{zs}^{eq}\gamma_{zs}\big)\,dsdz + \tag{15}$$
$$+ \frac{1}{3}t_e^3 \int_{H_e}\int_{L_e}\big(\delta\vartheta' \cdot G_{zs}^{SV,eq}\,\vartheta'\big)\,dsdz$$

where E_z^{eq}, G_{zs}^{eq} and $G_{zs}^{SV,eq}$ are equivalent moduli, taking into account single contributions of each material through the finite element thickness:

$$E_z^{eq} = \frac{1}{t_e}\sum_{i=1}^m E_z^i \cdot t_i \tag{16a}$$

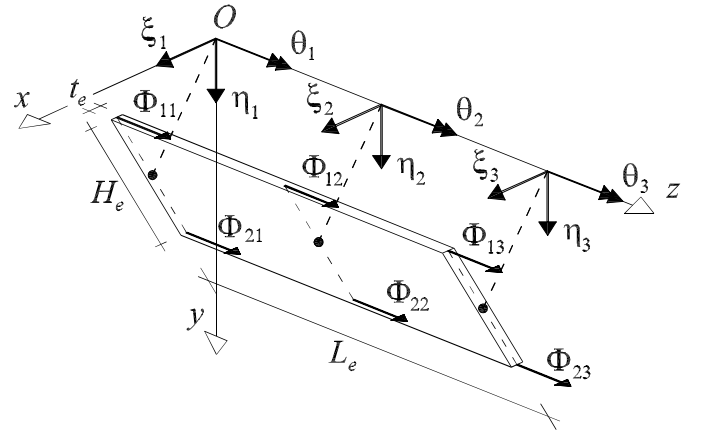$$G_{zs}^{eq} = \frac{1}{t_e}\sum_{i=1}^m G_{zs}^i \cdot t_i \tag{16b}$$

Figure 5. Finite element of *panel* type and corresponding dofs.

$$G_{zs}^{SV,eq} = \frac{4}{t_e^3}\sum_{i=1}^m G_{zs}^i\left(x_{n,i}^3 - x_{n,i-1}^3\right) \tag{16c}$$

Substitution of Equations 13, 14 into Equation 15, yields:

$$\delta L_{vi}^e = t_e E_z^{eq}\int_{H_e}\int_{L_e}(\delta\Phi^T\mathbf{N}_\phi')\,(\mathbf{N}_\phi'^T\Phi)\,dsdz +$$
$$+ t_e G_{zs}^{eq}\int_{H_e}\int_{L_e}(\delta\Phi^T\mathbf{N}_{\phi,s} + \alpha_x\delta\xi^T\mathbf{N}' + \alpha_y\delta\eta^T\mathbf{N}' + r\delta\theta^T\mathbf{N}')\cdot$$
$$\cdot(\mathbf{N}_{\phi,s}^T\Phi + \alpha_x\mathbf{N}'^T\xi + \alpha_y\mathbf{N}'^T\eta + r\mathbf{N}'^T\theta)\,dsdz + \tag{17}$$
$$+ \frac{1}{3}t_e^3 G_{zs}^{SV,eq}\int_{H_e}\int_{L_e}(\delta\theta^T\mathbf{N}')\,(\mathbf{N}'^T\theta)\,dsdz = \delta\mathbf{U}_e^T\mathbf{K}_e\,\mathbf{U}_e$$

where vector $\mathbf{U}_e^T = [\xi^T, \eta^T, \theta^T, \Phi^T]$ collects all dofs of the element and $\mathbf{K}_e$ is the corresponding stiffness matrix. Moreover, external virtual work is given by:

$$\delta L_{ve}^e = \int_{L_e}(q_x\delta\xi + q_y\delta\eta + m_t\delta\theta)\,dz +$$
$$+ \delta\xi^T\mathbf{Q}_x + \delta\eta^T\mathbf{Q}_y + \delta\theta^T\mathbf{M}_t \tag{18}$$

where:
- q_x, q_y, m_t are external distributed loads corresponding to rigid body cross-section displacements $\xi(z)$, $\eta(z)$, $\theta(z)$,
- $\mathbf{Q}_x^T = [Q_{x1}, Q_{x2}, Q_{x3}]$, $\mathbf{Q}_y^T = [Q_{y1}, Q_{y2}, Q_{y3}]$, $\mathbf{M}_t^T = [M_{t1}, M_{t2}, M_{t3}]$ are vectors of generalized applied forces associated with dofs ξ, η, θ.

Substituting Equations 8 in Equation 18 yields:

$$\delta L_{ve}^e = \delta\xi^T\mathbf{t}_\xi + \delta\eta^T\mathbf{t}_\eta + \delta\theta^T\mathbf{t}_\theta +$$
$$+ \delta\xi^T\mathbf{Q}_x + \delta\eta^T\mathbf{Q}_y + \delta\theta^T\mathbf{M}_t = \delta\mathbf{U}_e^T\mathbf{F}_e \tag{19}$$

where:

$$\mathbf{t}_\xi = \int_{L_e}\mathbf{N}(z)q_x\,dz, \qquad \mathbf{t}_\eta = \int_{L_e}\mathbf{N}(z)q_y\,dz,$$

$$\mathbf{t}_\theta = \int_{L_e} \mathbf{N}(z) m_t \, dz \tag{20}$$

and:

$$\mathbf{F}_e^T = [\mathbf{t}_\xi + \mathbf{Q}_x, \ \mathbf{t}_\eta + \mathbf{Q}_y, \ \mathbf{t}_\theta + \mathbf{M}_t, \ 0] \tag{21}$$

Setting $\delta L_{vi}^e = \delta L_{ve}^e$, under the assumption of arbitrary values of variations $\delta\xi$, $\delta\boldsymbol{\eta}$, $\delta\boldsymbol{\theta}$, for $0 \le z \le L_e$, Equations 17 and 19 yield:

$$\mathbf{K}_e \mathbf{U}_e = \mathbf{F}_e \tag{22}$$

stating equilibrium condition for the general finite element.

4 SOLUTION METHOD IN THE NON-LINEAR RANGE

When a reinforced concrete structure in the cracked range is considered, Equation 22 gives a non linear system of equations due to non linear behavior of concrete. A Newton-Raphson method has then been adopted to solve the non-linear FE problem. The solution algorithm originally proposed by Batoz & Dhatt (1979) has been used. This method enables step-by-step controlling of a single, monotonically growing dof, while shape of external load distribution is defined separately. All unconstrained dofs are unknown, except for the displacement component adopted as the control parameter; increment of load multiplier λ is also unknown. With this method, softening branches in load-displacement response (as in the case of crack formation in concrete under tension) can be correctly followed without imposition of the deformed shape to the structural element.

First, equation system stating equilibrium for the linearized Newton-Raphson problem is written. Then, in the usual way, partitioning of the system is operated, thus imposing boundary conditions on displacements. The following reduced equation system of order m can be obtained, being m the number of unconstrained dofs and with i indicating general Newton-Raphson iteration:

$$\mathbf{K}_i d\mathbf{U}_i = d\lambda_i \hat{\mathbf{F}} + \mathbf{R}_i + \mathbf{C}_i \tag{23}$$

where $\mathbf{K}_i$ is the structural tangent matrix, $\hat{\mathbf{F}}$ a constant vector determining the shape of external load distribution, $\mathbf{R}_i$ the vector of residual forces and $\mathbf{C}_i$ a vector originating from system partitioning. Moreover, $d\mathbf{U}_i$ and $d\lambda_i$ are variations of dofs vector and load multiplier, respectively. For each Newton-Raphson iteration i, the following equation system can be derived from Equation 23:

$$d\mathbf{U}_i = d\lambda_i \mathbf{U}^a + \mathbf{U}^b \tag{24}$$

where:

$$\mathbf{U}^a = \mathbf{K}_i^{-1} \hat{\mathbf{F}}, \quad \mathbf{U}^b = \mathbf{K}_i^{-1} (\mathbf{R}_i + \mathbf{C}_i) \tag{25a,b}$$

Equation system 24 must be solved for $d\lambda_i$ and $d\mathbf{U}_i$ for a given step increment $\Delta\bar{u}$ of the controlled dof. This is done easily, if j-th equation (corresponding to controlled dof) is extracted, stating:

$$\begin{aligned} d\lambda_i U_j^a + U_j^b &= \Delta\bar{u} \qquad \text{for iteration} \quad i = 1 \\ d\lambda_i U_j^a + U_j^b &= 0 \qquad\quad \text{next} \quad (i > 1) \end{aligned} \tag{26}$$

Increment $\Delta\bar{u}$ is imposed at the first iteration, as evidenced by Equation 26.

5 MODELIZATION OF PRESTRESSED REINFORCED CONCRETE

5.1 Constitutive laws for concrete

In the present study, concrete behavior in tension is considered linear up to tensile strength with softening branch after the peak stress. Shear deformability is considered purely elastic; beam is then supposed not to crack under shear stresses for service load levels.

A smeared crack law (Reinhardt & Yankelewsky 1989) has then been used for concrete in tension. The law is linear with elastic modulus E_c up to cracking occurring at point $[\varepsilon_{ct}, f_{ct}]$; softening branch is described by the following relationship between concrete stress σ_c and strain ε_c:

$$\sigma_c = f_{ct} \left(1 - \frac{\varepsilon_c}{\varepsilon_{c0}}\right)^2 \tag{27}$$

where ε_{c0} is value of strain where stress becomes zero. The complete constitutive law in tension (Fig. 6) is obtained by shifting Equation 27 to the right of the quantity ε_{ct}. Strain with zero value for stress becomes $\varepsilon_u = \varepsilon_{c0} + \varepsilon_{ct}$.

In compression a linear law with elastic modulus E_c is adopted, since service loads are considered.

5.2 Modelization of bars and pretensioning strands

For both pretensioning strands and steel bars, a linear elastic behavior is assumed. In the finite element model, the presence of ordinary steel bars is modeled as layers made of a different material. On the
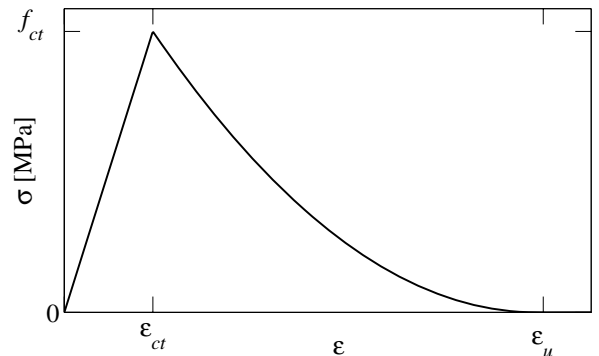
Figure 6. Reinhardt & Yankelewsky law (1988) for concrete in tension.

contrary, strands are modeled as a unique layer with different width.

Pretensioning is then introduced in the form of concentrated forces applied on strands at beam extremities.

6 RESULTS

Results of the non linear analysis on a simply supported, prestressed thin-walled beam are reported. Beam length is 24 m and cross-section is depicted in Figure 7. For beam geometry, see also Di Prisco et al. (1990). A uniformly distributed load q along beam length is applied. Overall pretensioning force is set to 2180 kN. Material parameters are listed in Table 1.

Modelization of the cross-section is shown in Figure 8; thickness of branches and main nodes of discretization are reported. Additional nodes have then been placed for bars and strands, as well as along section branches to improve the solution (see Fig. 10). Prestress load has been introduced from the beginning together with beam weight.

In a second stage, vertical load has been incremented by controlling increase of beam deflection, following the method described in Section 4; analysis has been carried out up to the attainment of compression strains (0.8‰) corresponding to about 40% of compressive strength (conventional limit of linear elastic behaviour). Cracking first occurs for a distributed load of about 8 kN/m. By increasing load level, beam stiffness in bending reduces significantly, as shown by slope decrease of the load-deflection curve in Figure 9. After an intermediate phase with cracking extending from middle-span, curve becomes approximatively linear. Due to the presence of prestress load, cracking is revealed by a very gradual change in stiffness, without softening branches as in the case of ordinary steel reinforcement only.

Figures 10a-d show the evolution of cracked region with load increase, expanding from middle-span. Black points indicate Gauss points where
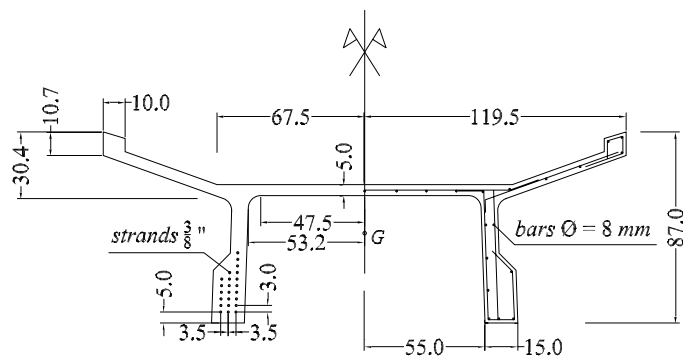

Figure 7. Beam cross-section with prestressing and ordinary reinforcement.
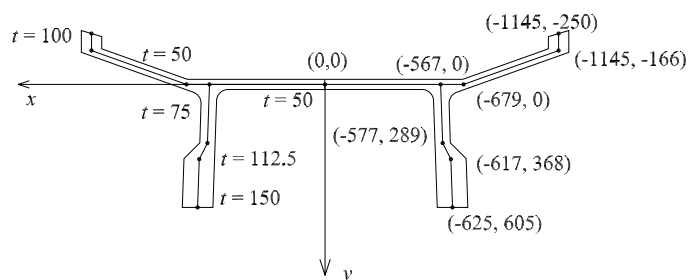

Figure 8. Modeling of cross-section: coordinates of main points (right) and thickness of branches (left).

strain overcomes the cracking limit ε_{ct}; moreover, black line indicates the neutral axis position (null axial strain). Having adopted a local model, strain localization in tension could be expected. Nevertheless, Figures 10 indicate a well distributed cracking state.

shows strain profile for three different load levels at the cross-section 48 cm far from middle-span. Moreover, for the same section, in Figure 12 normal stresses in concrete are reported, for different load levels. Softening behaviour of concrete in tension due to cracking in the bottom portion of the beam is shown.

7 CONCLUSIONS

A new finite element model is developed for non linear behaviour of concrete under service loads.

Table 1: Material properties.

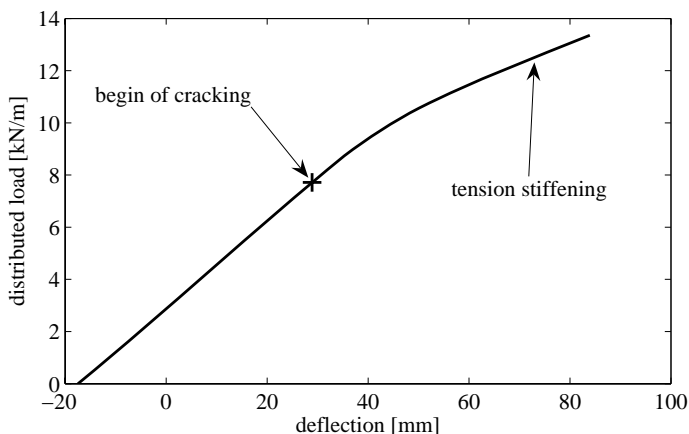| Property	Symbol	Value	Unit
Elastic modulus of concrete	E_c	40	GPa
Shear modulus of concrete	G_c	17.4	GPa
Tensile strength of concrete	f_{ct}	3.7	MPa
Ultimate strain of concrete	ε_u	0.5‰	GPa
Elastic modulus of steel strands	E_{sp}	196	GPa
Elastic modulus of steel bars	E_s	206	GPa
Shear modulus of steel strands	E_{sp}	75.4	GPa
Shear modulus of steel bars	E_s	79.2	GPa

Figure 9. Distributed load vs. deflection.
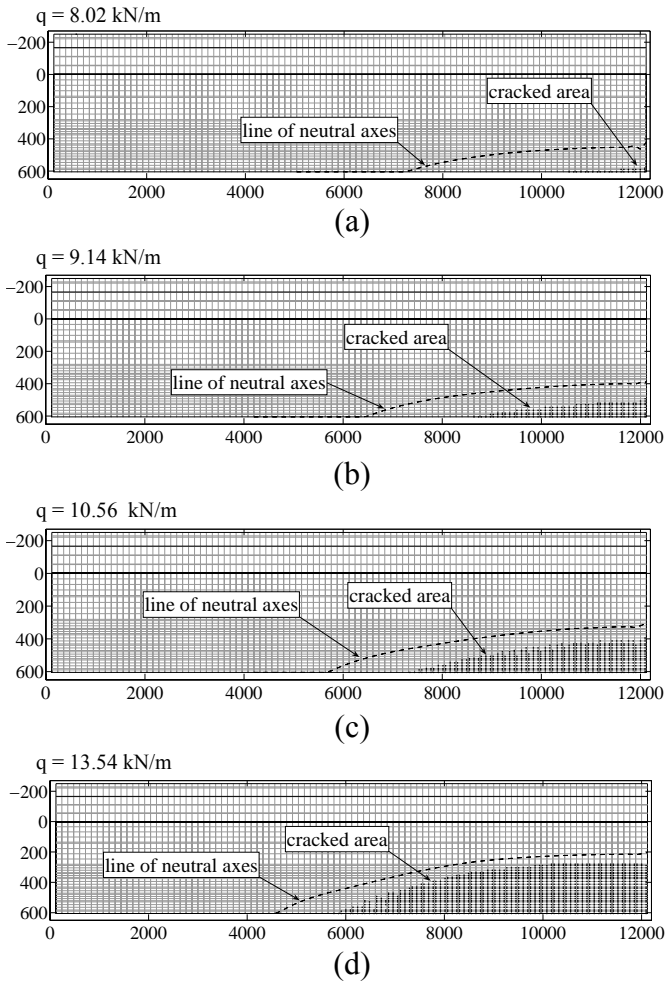
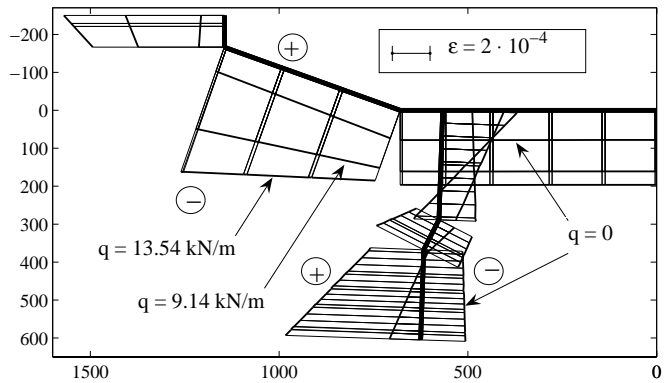Figure 10. Cracking configuration and line of neutral axes at different loading levels.

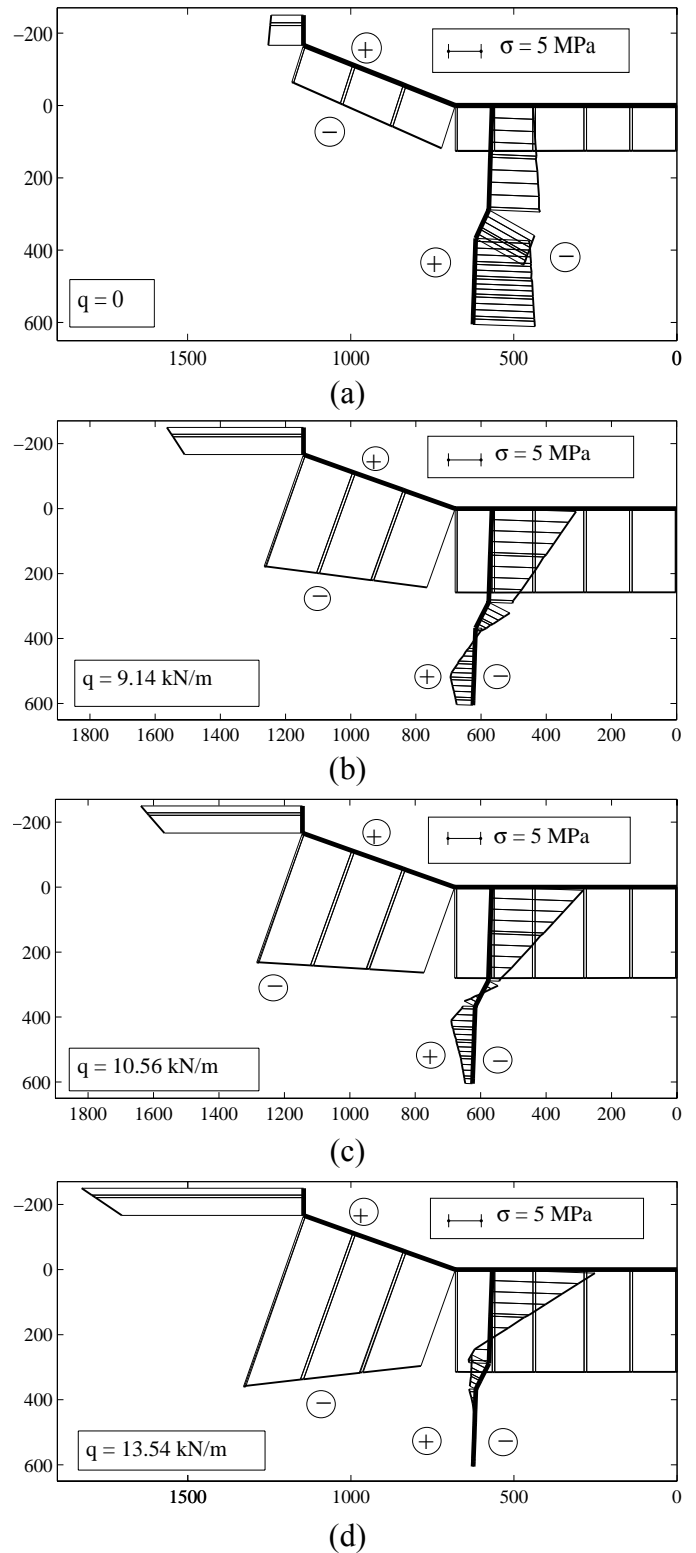Figure 11. Strains close to middle-span for different load levels.

Cross-sections are assumed rigid in their own planes, so reducing the number of dofs. Shear elastic deformability is considered into the model, though inelastic deformability due to cracking is only taken into account for normal strains. A smeared cracked model describes the average damaging behaviour.

In a future study, a non local constitutive model will be used to model cracking behaviour of concrete (Pijaudier-Cabot & Bažant 1986, Bažant & Cedolin 1991). Non local models are typically used as regularization techniques when strain localization occur in numerical analysis.

Moreover, the model will be extended to cover the case of long-term loadings, including creep deforma-

Figure 12. Stress distributions close to middle-span for different load levels.

tion of concrete and steel relaxation of prestressing strands. Since membrane deformation of individual panels only are considered (no out-of-plane bending), introduction of creep deformation according to solidification theory is much more effective and computationally efficient with respect to ordinary shell elements.

REFERENCES

Batoz, J.L. & Dhatt, G. 1979. Incremental displacement algorithms for non linear problems. *International Journal for Numerical Methods in Engineering* 14: 1262-1267.

Bažant, Z.P. & Cedolin, L. 1991. *Stability of Structures*. Oxford University Press.

Bažant, Z.P. (Ed.) 1988. *Mathematical modeling of creep and shrinkage in concrete.* John Wiley and Sons.

Bottoni, M., Mazzotti, C. & Savoia, M. 2006. A F.E. model for viscoelastic behaviour of composite pultruded shapes. *Proceedings of ECCM 2006*, Lisbon, Portugal.

Capuani, D., Savoia, M. & Laudiero, F. 1988. Dynamics of multiply connected perforated cores. *Journal of Engineering Mechanics*, *ASCE*, 124:622-629.

Di Prisco, M., Gambarova, P., Toniolo, D. & Failla, C. 1990. Sperimentazione su prototipo di un componente prefabbricato in c.a.p. per coperture di grande luce (in Italian). *Proceedings of CTE 1990*, Bologna, Italy.

Favre, R., Jaccoud, J.P., Burdet, O. & Charif, H. 1997. *Dimensionnement des structures en béton. Aptitude au service et éléments de structures -* Vol. 8 (in French). Presses Polytechniques et Universitaires Romandes.

Ghali, A. & Favre, R. 1994. *Concrete structures, stresses and deformations*, London: E & FN Spon Publisher.

Laudiero, F. & Zaccaria, D. 1998. A consistent approach to linear stability of thin-walled beams of open sections. *International Journal of Mechanical Sciences*, 30(8): 543-557.

Laudiero, F. & Savoia, M. 1990. Shear strain effects in flexure and torsion of thin-walled beams with open or closed cross-section. *Thin-Walled Structures*, 10: 87-119.

Prokič, A. 1996. New warping function for thin walled beams, I: Theory. *Journal of Structural Engineering*, *ASCE*, 122(12):1437-1442.

Prokič, A. 2002. New finite element for analysis of shear lag. *Computers & Structures*, 80:111-1024.

Pijaudier-Cabot, G. & Bažant, Z.P. 1986. Nonlocal damage theory, *Journal of Engineering Mechanics*, *ASCE*, 113(2): 1512-1533.

Reinhardt, H.W. & Yankelewsky, D.Z. 1989. Uniaxial behavior of concrete in cyclic tension, *Journal of Structural Engineering*, *ASCE*, 115(1): 166-182.